Archaeological and Anthropological Sciences (2024) 16:153
https://doi.org/10.1007/s12520-024-02062-w

BRIEF REPORT

A multi-technique approach to unveil the composition and fabrication of a pre-Roman glass masterpiece: a double-faced human-head shape polychrome glass pendant (2nd -1st c. BC)

S. Barroso-Solares[1,2,3] · E. Estalayo[4] · J. Aramendia[4] · E. Rodriguez-Gutierrez[1,2] · C. Sanz-Minguez[1,2] · A. C. Prieto[1,2] · J. M. Madariaga[4] · J. Pinto[1,2,3]

Received: 9 April 2024 / Accepted: 20 August 2024 / Published online: 30 August 2024

Abstract

Pre-Roman glass craftsmanship reached its summit with the development of complex polychrome glass beads, being the Phoenician glass pendants the most exquisite and elaborate example. The uniqueness and complexity of such findings could reveal key information for the understanding of the production and trade of glass pieces at that age. However, these findings have practically never been studied from a physic-chemical perspective. In this work, a remarkable polychrome glass pendant (2nd -1st c. BC) found at the archaeological site of Pintia (Padilla de Duero, Valladolid, Spain) is studied by a multi-analytical non-destructive approach, employing X-ray tomography to understand its fabrication procedure, as well as X-ray fluorescence (XRF) and Raman spectroscopy, both employed in microscopic mode, to determine the composition of each glass employed in its fabrication. The outstanding preservation state and well-defined archaeological context of this glass pendant offered a unique opportunity to expand the understanding of pre-Roman glass pieces, while the combination of the experimental techniques employed provided the first complete and detailed study of a Phoenician glass pendant. The fabrication procedure of the pendant has been identified step-by-step, showing evidence of the use of pre-made pieces for the eyes, as well as hints of its fabrication in a secondary workshop. Moreover, the microchemical analysis of the vividly colored glasses by XRF and Raman spectroscopy revealed a composition compatible with the use of natron as fluxing agent, typical of Phoenician glass, the presence of surface alterations corresponding to carbonatation processes, as well as the nature of the employed chromophores or pigments: Mn, Cu, and Co for the blue, Fe-S for the black, $CaSb_2O_7$ and $CaSb_2O_7 + TiO_2$ for two diverse white glasses, and a pyrochloric triple oxide ($Pb_2Sb_{2-x}Sn_xO_{7-x/2}$) and lead oxides for the yellow. Remarkably, the use of pyrochloric triple oxides as yellow pigments has scarcely been previously reported at that age. Finally, the identification by Raman spectroscopy of $CaSb_2O_7$ and the β-phase of $CaSiO_3$, as well as the Raman spectra features of the glass matrix corresponding to the blue glass, indicated maximum firing temperatures below 1100 °C.

Keywords X-ray fluorescence · Raman spectroscopy · X-ray tomography · Phoenician · Iberian Peninsula

✉ J. Pinto
javier.pinto@uva.es

1 Archaeological and Historical Materials (AHMAT) Research Group, Condensed Matter Physics, Crystallography, and Mineralogy Department, Faculty of Science, University of Valladolid (UVa), Valladolid, Spain

2 Centro de Estudios Vacceos "Federico Wattenberg", Faculty of Philosophy and Literature, University of Valladolid, Valladolid, Spain

3 BioEcoUVA Research Institute on Bioeconomy, University of Valladolid (UVa), Valladolid, Spain

4 Department of Analytical Chemistry, University of the Basque Country (UPV/EHU), Bilbao, Spain

Introduction

Although nowadays a common product, glass was considered a most valuable material during the Protohistory (Seefried 1979, 1982). The invention of glass in Mesopotamia is generally assumed to have occurred around 2500 BC, although the starting of the actual glass production is widely accepted about 1600 BC (Gratuze 2013). However, this material was rare until the end of the Bronze Age, becoming common during the Iron Age and widespread along the Mediterranean from the primary production sites at

Syria-Palestine and Egypt (Gratuze 2013). In particular, Phoenicians are considered to play a key role in the production and distribution of glass during the first millennium BC, although there is still no certainties about the glass production model in place during that age, as well as the existence and location of primary and secondary workshops (Costa et al. 2021).

Among the most exquisite pre-Roman polychrome glass beads, the Phoenician glass pendants, the summit of glass craftsmanship at that age, should be highlighted. These objects generally can only be found in the collections of a few remarkable museums, as they are scarce. Generally speaking, Carthage is where more glass pendants have been recovered, and it has been proposed as a main glass production center since the 4th century BC (Seefried 1979, 1982).

The work of M. Seefried, developing a detailed catalog and classification for such pieces, reported over 600 glass pendants in the entire Mediterranean area, generally found in tombs and a large number, about 118, concentrated in the Tunisian museums (Seefried 1982). As a comparison, only in the context of the Iberian Peninsula and Balearic Islands, about 18 000 pre-Roman glass beads have been recovered (own data). Accordingly, just about ten glass pendants, 12 according to our accounting, have been found in the same territory (Ávila 2011). The ratio between glass pendants and the rest of glass beads, less than one to one thousand, clearly indicates their unique and high prestige character (i.e., if glass beads were already a prestige good at that age, these pieces would only have been available to the highest-ranking elites, particularly far from the production workshops).

Among the pre-Roman glass pendants recovered in the Iberian Peninsula, a remarkable example was found at the archaeological site of Pintia (Padilla de Duero, Valladolid, Spain) (Fig. 1, see the Experimental section for more details)(Pinto et al. 2020). This archaeological site has produced one of the most important collections of pre-Roman glass beads in the interior of the Iberian Peninsula, reaching over 1 000 pieces. As there is no proof that the local culture inhabiting Pintia, the Vaccaei, had the technical capabilities to produce glass pieces, the large number of recovered glass pieces and the presence of this extraordinary glass pendant suggest strong commercial and political relationships with Mediterranean cultures.

Relevant information can be obtained from ancient glasses using diverse experimental techniques. For instance, Raman spectroscopy can identify the characteristics of the glass network and relate them with the manufacturing procedure of the glass piece and even its composition, following a procedure proposed by Ph. Colomban (Colomban 2003, 2013; Colomban et al. 2004, 2006; Oikonomou et al. 2008). Moreover, it is a powerful technique to identify the pigments incorporated into the glass precisely (Bouchard and Smith 2003; Ricciardi et al. 2009; Sánchez et al. 2012; Colomban 2019). In addition, techniques capable of providing the elemental composition of the glass have been extensively employed to study ancient glasses. High accuracy and low detection limits are generally achieved by techniques such as Laser Ablation – Inductively Coupled Plasma – Mass Spectrometry (LA-ICP-MS) (Devulder et al. 2015; Van Strydonck et al. 2018; Truffa et al. 2019; Rolland and Venclová 2021), X-Ray Absorption Fine Structure (XAFS) spectroscopy (Pinakidou et al. 2020), X-ray absorption near edge structure (XANES) (Quartieri et al. 2005), or ion beam-based techniques such as Particle Induced X-ray and

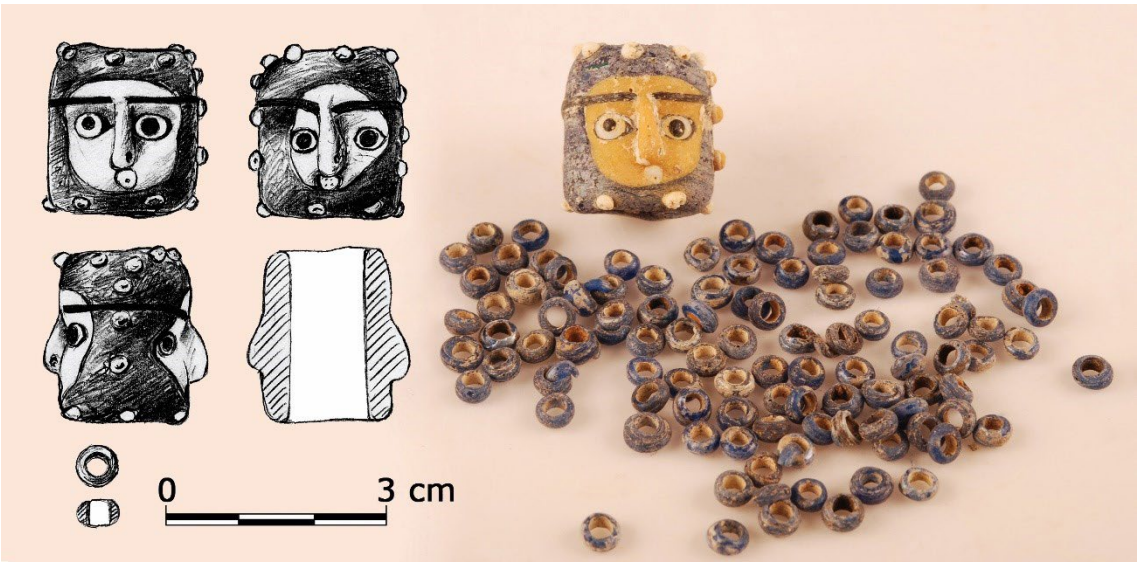

Fig. 1 Double-faced human-head shape polychrome glass pendant (2nd -1st c. BC) recovered at Pintia (Valladolid, Spain) (Reference: sample 5422). Reproduced with permission from: C. Sanz-Minguez & J. C. Coria-Noguera (2018) (Sanz-Minguez and Coria-Noguera 2018)

Gamma Emission (respectively PIXE and PIGE) (Mathis et al. 2010; Constantinescu et al. 2018; Šmit et al. 2020). Also other more accessible and non-invasive techniques such as scanning electron microscopy (SEM) equipped with energy-dispersive X-ray (EDX) analyzers (García-Heras et al. 2005; Pinto et al. 2020; Medeghini et al. 2022). X-ray fluorescence (Jokubonis et al. 2003; Rosi et al. 2011; Dong et al. 2020; Micheletti et al. 2020) can be employed with this aim, although providing slightly higher detection limits, particularly in the case of EDX. The analysis of the elemental composition of ancient glasses allows their classification (Gratuze 2013; Henderson and Henderson 2013), and even, in some cases, can provide hints about the provenance of the primary glasses or pigments and chromophores according to the ratios between certain elements (e.g., Co/Zr, Sr/Ca, Sr/Zr) when the techniques with the lowest detection limits are employed (Van Strydonck et al. 2018; Truffa et al. 2019; Rolland and Venclová 2021). Last but not least, the use of X-ray tomography has revealed as an essential tool for the study of complex polychrome glass beads, providing valuable information about their manufacturing procedure and even glass corrosion (Bertini et al. 2014; Cheng et al. 2019; Zhang et al. 2020; Nykonenko et al. 2023; Franceschin et al. 2024).

Particularly, the combination of several experimental techniques, normally including spectroscopy and elemental composition analysis techniques, have been successfully employed for the study of archaeological glass beads (Sánchez et al. 2012; Costa et al. 2019b, c; Dong et al. 2020).

Regarding the glass pendants, the expertise required to make these pieces limits their production to highly specialized workshops, leading to the classification proposed by M. Seefried for their chronology and potential provenance based on their morphology and characteristics, but without any additional information from an archaeometric point of view (Seefried 1979, 1982). Consequently, an extensive archaeometric analysis of this type of samples could provide a unique opportunity to obtain information on the characteristics of the glasses used in different workshops and chronologies. However, just six of more than six hundred glass pendants recovered in the Mediterranean have been partially studied using some of the abovementioned techniques.

Three polychrome glass pendants recovered from Mozia island (8th -6th c. BC, Sicily, Italy) have been studied by X-ray powder diffraction and electron microprobe analysis (Arletti et al. 2012). It was proposed that the blue color was achieved in one of the pendants by the combination of Cu and Co, whereas in the other two, it was achieved by high levels of Fe. In the case of the yellow regions, the presence of PbO and Sb_2O_3 is highlighted, being confirmed by X-ray diffraction the presence of $Pb_2Sb_2O_7$. According to the obtained results, a Phoenicia-Punic origin was proposed for these pendants (Arletti et al. 2012). In addition, a well-preserved pendant recovered from Nora cemetery (7th -6th c. BC, Sardinia, Italy) has been studied by SEM-EDX, LA-ICP-MS, and Raman spectroscopy, suggesting a Levantine origin and the use of natron as fluxing agent, as well as the use of Fe in the dark blue-green glass and $CaSb_2O_6$ for the white glass (Bettineschi et al. 2020; Malaman et al. 2024). Moreover, a pendant from the Marchetti Collection was studied following the same approach, suggesting it could be a forgery (Malaman et al. 2024). Also, preliminary results about the glass pendant studied in this work were published together with the analysis of the blue glass beads next to which it was found, as well as other conventional glass beads (Pinto et al. 2020). The information provided suggested a potentially diverse origin for the pendant and the other glass beads, as well as highlighted that the complexity, uniqueness, and richness of the glass pendant required further work and complementary experimental techniques. In particular, deepening the analysis of this piece is the aim of this work.

Herein, the first complete and comprehensive archaeometric analysis of an extraordinary well-preserved pre-Roman glass pendant, specifically of the one recovered at Pintia (Valladolid, Spain), is presented. The complementary use of X-ray tomography, X-ray fluorescence, and Raman spectroscopy has revealed hidden details about its manufacturing process, identified the pigments employed in each glass composing the pendant (some unexpected at that time), and provided evidence about its probable fabrication in a secondary workshop.

Experimental

Sample description and context

The studied sample (ref.: sample 5422) is a glass pendant, a polychrome cylindrical glass bead with an external diameter of about 23 mm, internal diameter of about 12.5 mm, and height of about 26.7 mm (Figs. 1 and 2). It was recovered from a closed context in tomb 144 of the “Las Ruedas” necropolis at Pintia (necropolis location: 41°37’07.8"N 4°10’09.8"W, Valladolid, Spain) in the excavation campaign carried out in 2007. This tomb presented 1.5 m of diameter, and its base was found 1.8 m below the surface, being located in the G2h2 sector of the necropolis, corresponding to the 2nd-1st centuries BC (Sanz-Minguez and Coria-Noguera 2018). The content of the tomb was well-preserved, including dozens of objects and an exceptional vitreous necklace composed of more than one hundred blue glass beads and the glass pendant. Considerations about

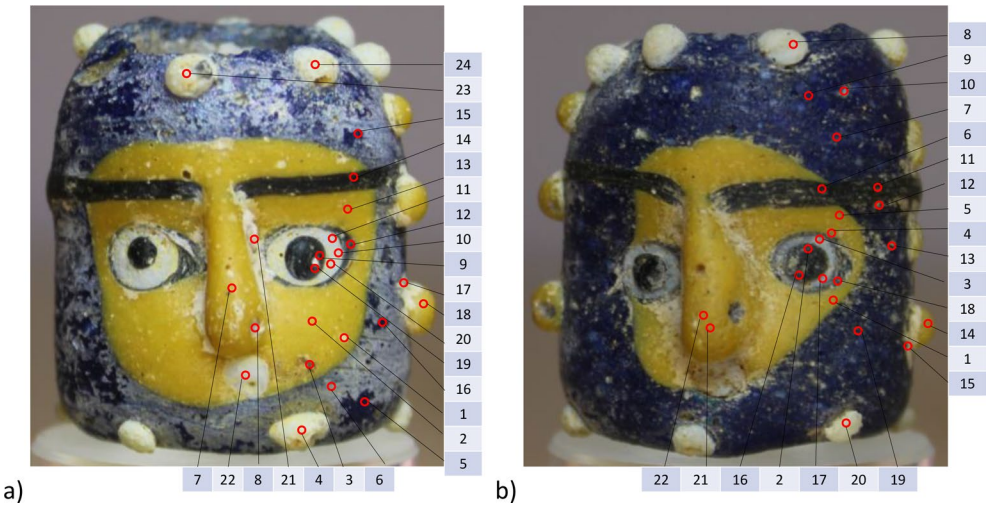

Fig. 2 Analyzed points in faces A (**a**) and B (**b**) of the glass pendant

the elements found as trousseaus and viatic offerings could indicate that the tomb corresponds to a young woman, who could have been originally from the Iberian people (Sanz-Minguez and Coria-Noguera 2018).

The glass pendant presents two human faces designed with four colors: blue, yellow, white, and black (Figs. 1 and 2). The blue glass is smooth and represents the hair and beard, while the yellow glass delimited the faces. Both faces present prominent noses and depressed areas corresponding to the eye sockets and mouth. The eyes are composed of a white sclera and a black pupil (i.e., the iris is not represented), surrounded by a black eye-line. The eye-browns are represented by a continuous black line, only interrupted below the nasal bridge in both faces. The mouths correspond to white depressed circles below the noses. Two vertical side-lines of three yellow balls separate the faces, whereas the top and bottom borders of the bead present six white balls (one of them has been lost).

The characteristics, chronology, and morphology of the glass pendant clearly correspond to the F_1 classification proposed by M. Seefried, also known as *perles masques* (e.g., beads with masks) (Seefried 1979, 1982). This kind of ancient glass pendants is characterized by the average size and all the design and decorative elements previously described for the studied glass pendant. According to M. Seefried, this is the only kind of glass pendants that does not present a suspension ring. These pieces are supposed to be fabricated around a sand and clay core, over which successive glass layers with different colors were applied. A new layer was applied over the first and thicker layer, forming the contour of the faces. It is proposed that, on this new layer, the craftsman modeled by pressure the eye sockets, then placed a piece of glass to form the nose, then a rod forming the eye-browns, and finally three successive layers of glass filling the eye sockets and a small glass piece as mouth to complete each face (Seefried 1979, 1982; Bettineschi et al. 2020). Moreover, small glass balls were placed around the pendant, and then the pendant was annealed to solidify and the core was removed (Seefried 1979, 1982). Summarizing, the manufacturing procedure is supposed to be based on the successive addition and sculpting of melted glass drops.

Among all the F_1 glass pendants recovered, M. Seefried only reported four samples with some chronological context: two pendants from Cumes (Italy) recovered in a tomb from the 5th century BC, and two pendants recovered at Carthage (Tunisia) whose chronology range is about 4th-2nd c. BC. Accordingly, it is proposed that the production of F_1 pendants started in the 5th century BC, and their use extended until the 2nd century BC. This chronology is in good agreement with those of the tomb from which the studied glass pendant was recovered (2nd-1st c. BC), being the studied pendant one of the few F_1 pieces with well-defined chronology. Almost half of the 44 F_1 glass pendants catalogued by M. Seefried have a known origin. From Carthage, four recovered F_1 pendants are reported, five from Cumas (Italy) and another two in Italy, one from Ibiza (Spain), one from Cyprus, and about ten around the Caucasus and nearby regions (Seefried 1979, 1982). More recent works conclude that glass pendants showing several faces appear more frequently in central, southeastern, and eastern Europe (Čelhar and Kukoc 2014). Moreover, less than ten of the cataloged F_1 glass pendants were found in an excellent state of preservation, such as those of the sample studied in this work. Also, it is reported that these pendants can present two or three faces, being the presence of three faces more common (Seefried 1979, 1982).

Accordingly, the glass pendant recovered at Pintia (Spain) represents a unique archaeological find, being one of the very few contextualized and exceptionally preserved F_1 glass pendants known and the only one found in the Iberian Peninsula (i.e., the westernmost recovered sample).

Experimental techniques

X-ray tomography was performed with a GE PHOENIX V|TOME|X S 240 (GE Measurement and Control, Billerica, MA, USA). These analyses/experiments were performed in the Microscopy and Microcomputed Tomography laboratory at CENIEH facilities in collaboration with CENIEH staff. 1800 projections of the samples were obtained with a voxel size of $20 \times 20 \times 20$ µm^3 and the following parameters: voltage and amperage of 120 kV and 135 µA, respectively.

The elemental composition and distribution of the glass pendant were studied by using the benchtop M4 TORNADO Energy Dispersive X-ray Fluorescence spectrometer (Bruker Nano GmbH, Berlin, Germany). This instrument is equipped with a micro-focus side window Rhodium X-ray tube powered by a low-power HV generator and cooled by air. The Rh X-Ray tube can work at a maximum voltage of 50 kV and at a maximum current of 700 µA. The spectral acquisitions in this work were performed at 40 kV of voltage and 600 µA of current. This equipment can work using polycapillar lenses, which allow performing both single point measurements down to 25 µm of lateral/spatial resolution, and Hyper Maps to determine the distribution of each element detected in the collected fragments. An XFlash® silicon drift detector with 30 mm^2 sensitive area and energy resolution of 145 eV for Mn-K_α was used for fluorescence radiation detection. In order to improve the detection of the lightest elements ($Z < 11$), filters were not used, and measurements were acquired under vacuum (20 mbar). The vacuum was achieved with a diaphragm pump MV 10 N VARIO-B. XRF maps were performed in 700 s and 2 cycles. The live time used for each single point measurement was 100 s. Two video-microscopes were used to focus the area under study, a low magnification (1 cm^2 area) one for the exploration of the sample and a higher magnification one (1 mm^2 area) for the final focusing, being the micrographs of the analyzed areas recorded. In order to obtain the Hyper Maps, the K_α or L_α line of each element was used after a previous elemental assignation and deconvolution of the spectral information using the M4 TORNADO software (Bruker Nano GmbH, Berlin, Germany). Both general elemental composition maps of the faces of the glass pendant and detailed point analysis were carried out.

A high-resolution Horiba-Jobin Yvon LABRAM HR 800 UV Raman spectrometer, with solid-state laser (532.8 nm), an Olympus BX41 microscope, and a Symphony CCD detector, was employed to study the glass pendant by Raman spectroscopy in microscopic backscattering mode with 100x magnification. Measurements were carried out for 120 s and two accumulations (higher accumulation numbers were attempted without an improvement of the obtained spectra), whereas the system was calibrated with the ν (Si-Si) mode at 521 cm^{-1}. The glass network was analyzed using Raman spectroscopy using the simplified dynamic vibrational Raman model proposed by Ph. Colomban (Colomban and Treppoz 2001). This model proposes a classification of glasses regarding their polymerization index (I_P), which is related to the average coordination degree of the Si tetrahedra on the glass network. In particular, I_p can be obtained as the ratio of the integrated intensities of the Raman δ (Si-O) bending bands centered at around 500 cm^{-1} (A_{500}), and the ν (Si-O) stretching bands centered at around 1000 cm^{-1} (A_{1000}). Moreover, the I_P has been related in previous works to the firing temperature employed in the production of ancient glasses, providing valuable information about the technological level involved in their production (Colomban 2003).

X-ray fluorescence and Raman spectroscopy were employed as complementary techniques by performing a detailed point-by-point analysis of the sample. In particular, 20 and 22 points were analyzed by both techniques at a microscopic scale in faces A and B, respectively (Fig. 2). Moreover, four additional points (21 to 24) were analyzed in face A by XRF to improve the statistical significance of the analysis of white glass in that face.

Results

X-ray tomography was employed to determine the inner distribution of each colored glass along the glass pendant, aiming to provide evidence about its fabrication procedure (Fig. 3). The analysis of the X-ray radiographs corresponding to each of the acquired projections to perform the three-dimensional reconstruction already provided useful information (Fig. 3.b and Video S1, see Supplementary Information). As the grayscale on X-ray radiographs depends on the density and/or the presence of heavy atoms, it is clear that the yellow glass is denser than the rest (Fig. 3.b). Moreover, black and blue glasses should be quite similar, as they do not provide significant contrast (e.g., the black line corresponding to eye-browns cannot be differentiated from the blue matrix, Fig. 3.a and 3.b). Therefore, it can be expected that there will be a similar elemental composition for both glasses, with relatively small amounts of diverse chromophores. Also, the balls located at the upper and lower ends of the pendant seem different from those located along the sides (Fig. 3.b). Finally, the visualization of the projections (Fig. 3.b and Video S1, see Supplementary Information) suggests that the eyes present a regular almost hemispherical shape within the glass matrix of the pendant.

The 3D tomographic reconstruction (Fig. 3.c and Video S.2, see Supplementary Information) confirmed the previous observations, providing additional details about the

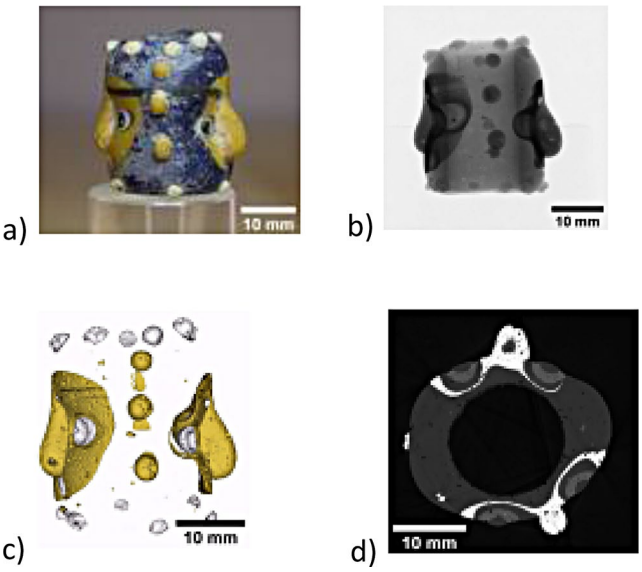

Fig. 3 Picture of the glass pendant (**a**) and corresponding projection (i.e., X-ray radiograph) obtained at this orientation (**b**). 3D tomographic reconstruction showing only the yellow and white glasses (**c**). Cross-section of the 3D tomographic reconstruction showing the inner structure of the eyes (**d**)

eyes. Both the black pupil and the white sclera are formed by regular almost hemispherical pieces. On the contrary, both the black glass surrounding the eyes and the yellow glass corresponding to the faces present no regular shapes within the pendant glass matrix (Fig. 3.c and Video S.2, see Supplementary Information). This is clearly evidenced in the cross-sections obtained from the 3D tomographic reconstruction (Fig. 3.d and Video S.3, see Supplementary Information. It should be noticed that in the cross-sections, lighter colors within the sample indicated higher X-ray absorption). While the thickness of the black pupil and white sclera keep constant proportions for any cross-section including the eyes, the black surrounding glass (i.e., eye-line) and the yellow glass of the faces below the eyes are irregular (Fig. 3.d, Figure S.1 and Video S.3, see Supplementary Information). Notably, the black glass is almost missing below the white sclera at some points, whereas in others, this black glass infuses into the yellow glass below the surface (Figure S.1, see Supplementary Information).

The results are in general consistent with the expected fabrication route for this kind of glass pendants (see Experimental section). The blue glass was shaped around a sand core, and then the yellow glass was placed and modeled in a molten state over the molten blue glass (Fig. 4). Then the black glass corresponding to the eye-line was also placed in a molten state over the yellow glass, maybe over already modelled eye sockets. On the contrary, the eyes are expected to have been previously fabricated by casting into hemispherical molds (i.e., first the black pupil and then the white sclera, with the pupil placed while the sclera was molten). This procedure using molds has been previously proposed in the literature for other glass beads (Cheng et al. 2019), being consistent with the regular shapes shown by the sclera and pupil and simplifying the production process of the pendants. Moreover, the pressure induced by placing the rigid

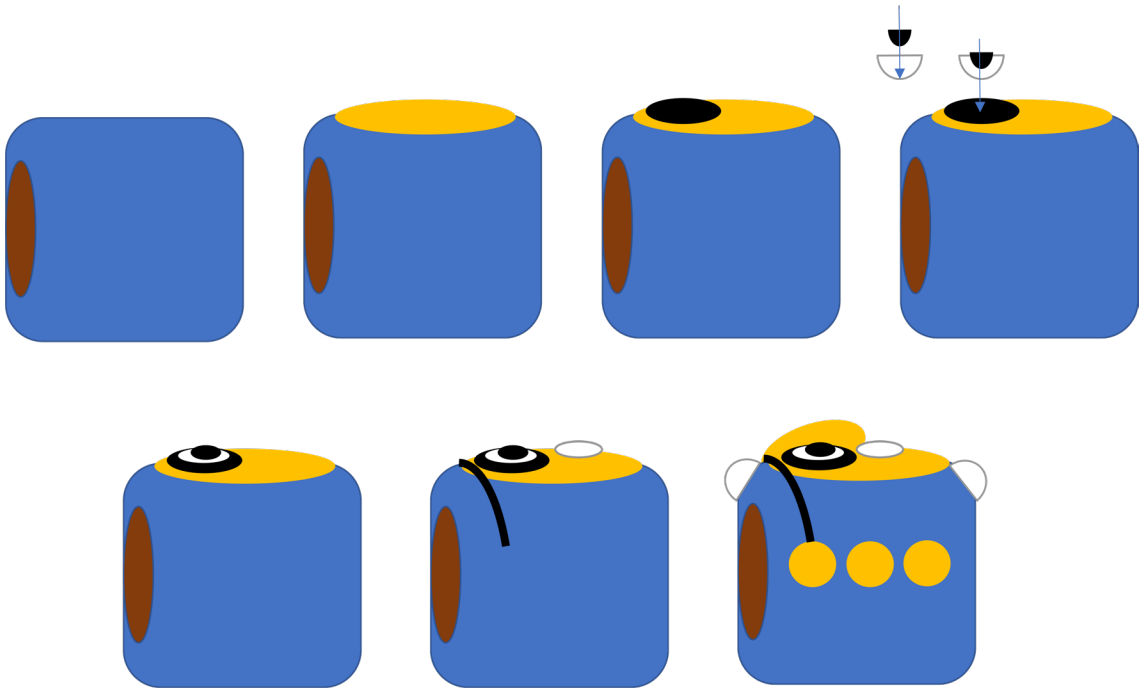

Fig. 4 Scheme of the glass pendant fabrication procedure proposed from the X-ray tomography results (only one face is showed, the procedure is expected to be carried out almost simultaneously in both faces)

hemispheric eyes into the molten black and yellow glasses explains their irregular shape and thickness below the eyes, as well as the flow of the black glass into the yellow one below the surface (Fig. 3.d, Figure S.1.a, and Video S.3, see Supplementary Information). These results enlighten and precise the previously proposed production route, in which the eyes were proposed to be modeled from successive layers of molten glass directly on the eye sockets (Seefried 1982).

Then, the black eye-lines and white mouths should have been placed before the nose, as the eye-browns rod and white spots corresponding to the mouths lie below the noses (Fig. 3.c, Figure S.1.b, and Video S.2, See Supplementary Information). Also, the nose appears also covering in some regions the black glass of the eye-lines (Fig. 3.d and Video S.3, see Supplementary Information), which is consistent with the addition of the nose on top of the face once the eyes and eye-browns are placed. At previous stages of the study of this piece, it was assumed that the nose was formed by pulling the molten yellow glass with tweezers, as both noses showed marks compatible with this manipulation (see on the left side Fig. 3.a and 3.c). However, the evidence provided by X-ray tomography proved that the noses were placed as additional pieces on top of the faces, probably by the use of tweezers while they remained molten. Finally, although poorly preserved in some cases, the white and yellow balls placed around the pendant also present a quite regular shape, which could be compatible with the use of molds. However, no signs of pressure from the placement of solid pieces into a molten glass matrix are found in this case (i.e., the interface between the balls and the blue glass matrix seems perfectly flat and follows the contour of the external surface of the pendant). Therefore, these balls could have been applied as molten glass drops directly on the surface of the pendant. A complete scheme of the fabrication process of the glass pendant is shown in Fig. 4. As the blue glass matrix should be in a molten state to allow the incorporation of the other glasses, both faces should have been modeled almost simultaneously.

In addition, it should be mentioned that before the X-ray tomography, it was not clear if all the balls could have been identical, composed of a yellow core and some kind of white covering, as some of the balls placed on the sides appear to have remains of that covering (Fig. 3.a). However, the obtained results evidence that the diverse nature of the balls, being composed only by white or yellow solid glasses.

Other features of the glass matrix can be identified on the cross-sections from the 3D tomographic reconstruction, such as impurities inside the glass matrix (e.g., white spots in Fig. 3.d) as well as gas bubbles (Fig. 3.d, Figure S.1, and Video S.3, see Supplementary Information) which are typically found in ancient glass beads (Wang et al. 2020). A detailed observation of the bubbles indicated that, although the majority are spherical, in the regions underneath the eyes (i.e., pupil and sclera), elongated bubbles on the yellow glass, as well as interfacial bubbles between the yellow glass and both the blue and black glasses are found (Figure S.1.c). Interfacial bubbles can only form when both glasses come into contact in a molten state, whereas the elongation of the bubbles indicated the existence of pressures perpendicular to the elongation direction during the fabrication procedure (e.g., the insertion of the pre-made glass eyes) (Wang et al. 2020). It should be noted that these observations fully support previous evidence and the proposed manufacturing process (Fig. 4).

As explained before, the contrast difference provided in X-ray tomography are directly related to the composition of the glasses. Thus, once the glasses present on the glass pendant and their distribution were clearly identified, their elemental composition was analyzed using X-ray fluorescence.

The first step was to perform an elemental mapping of both faces of the pendant (Fig. 5 and Figure S.2), aiming to provide qualitative information and evidence about the distribution of elements of interest. As expected, basic elements of the glass matrix, such as Si, Na, Al, K, and Ca can be found in all the glasses. However, Na is poorly detected, probably due to superficial de-alkanilization processes (Zanini et al. 2023a), and the yellow glass seems to present a slightly lower relative amount of Si, Al, K, and Ca regarding the other glasses. Assuming that the obtained Na values are lower than those of the original composition of the glass, these glasses correspond to the so-called low magnesium soda-lime silica glass produced using natron (Costa et al. 2021). Particularly, the presence of S in most of the glasses and those of Cl in all of them is compatible with the use of natron as a fluxing agent (Costa et al. 2021).

Moreover, high concentrations of Ca are found in the alterations around the nose, as well as on the white spots present on the pupils of the face A. Then, the blue glass is characterized by a higher relative presence of Mn, Cu, and Co regarding the other glasses, while the yellow glass is clearly characterized by the presence of Pb, and the black and white glasses by the presence of Fe and Sb, respectively (Fe can also be found in the alterations of the sample). Other elements, such as Cl, Mg, and Ti seem to be almost homogeneously distributed, whereas in the yellow glass the presence of Sn and Sr seem to be higher and lower than in other glasses, respectively.

The accuracy of this qualitative analysis was further confirmed by the results provided by the point analysis carried out in both glasses (Tables 1 and 2, and Tables S.1, S.2, S.3, and S.4, see Supplementary Information). The lower relative presence of some elements in the yellow glass, such as Si, is directly related to a high content of Pb (up to 31.5 (face A)

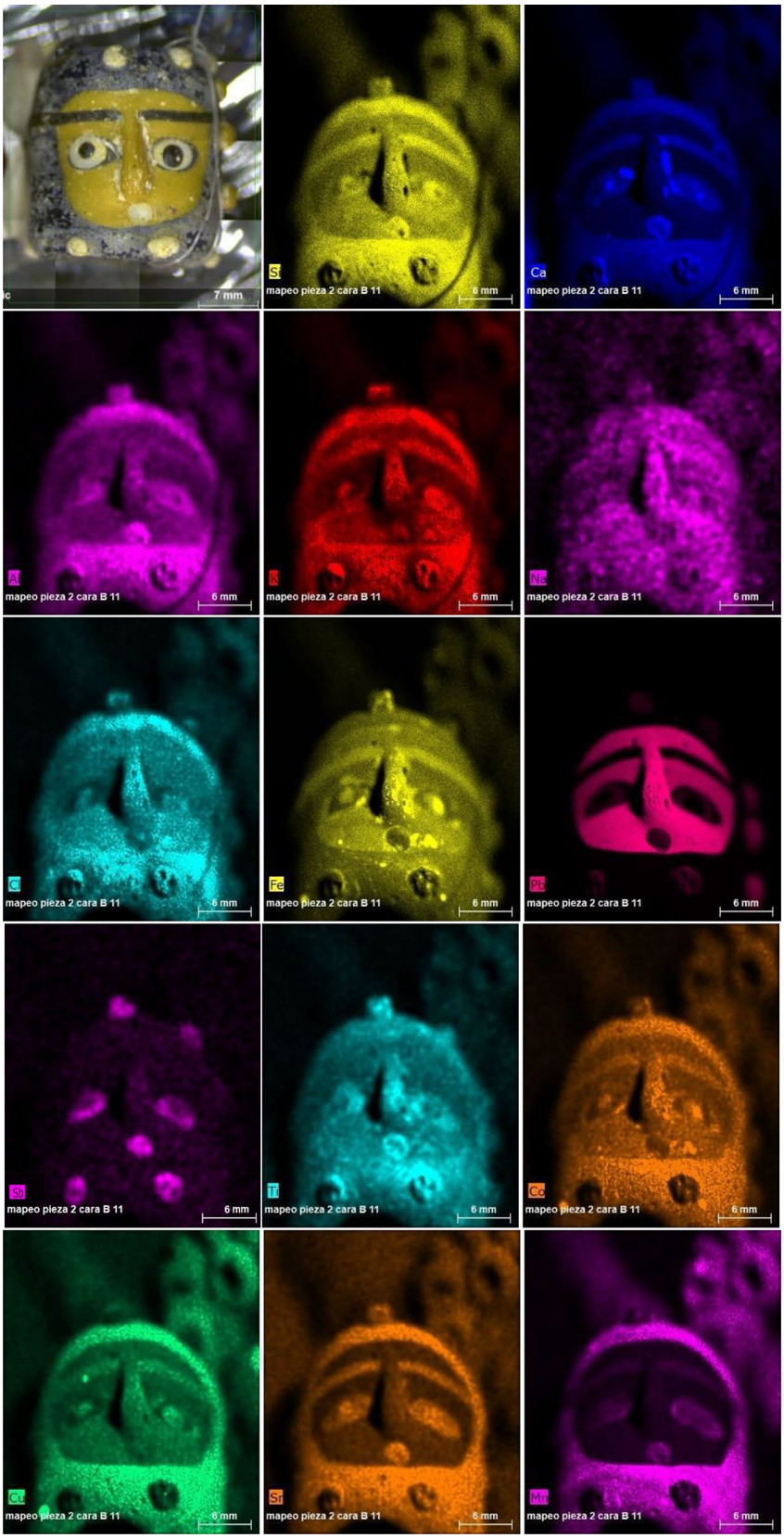

Fig. 5 ED-XRF maps of face A of the glass pendant

Table 1 XRF average composition of oxides (wt%) of the glasses composing face A of the glass pendant. The LOD is about an average of ± 0.01% for trace elements. Other elements, such as Cr, Ni, and V, were not found in concentrations above the detection limit. The concentration values indicated should be taken with caution since the matrix effect has not been taken into account; they should be considered semiquantitative. Although the order of magnitude is correct

Oxide \ Glass	Blue (wt%)			Yellow (wt%)			Black (wt%)			White-Eye (wt%)			White-Ball (wt%)		
SiO_2	64.6	±	4.8	40.9	±	4.4	57.5	±	3.4	58.4	±	3.0	47.1	±	3.9
Na_2O	4.2	±	1.4	4.7	±	1.1	5.5	±	2.1	2.0	±	0.2	1.8	±	0.8
K_2O	3.2	±	0.9	2.9	±	0.6	4.0	±	0.2	3.1	±	0.3	2.7	±	0.6
CaO	13.0	±	0.8	7.0	±	0.7	15.4	±	4.0	11.7	±	0.3	10.8	±	2.0
MgO	0.16	±	0.17	0.3	±	0.2	0.42	±	0.09	0.6	±	0.1	0.00	±	0.00
MnO	0.94	±	0.15	0.02	±	0.01	0.24	±	0.07	0.27	±	0.02	0.32	±	0.05
CuO	0.31	±	0.06	0.06	±	0.01	0.17	±	0.03	0.05	±	0.01	0.05	±	0.01
PbO	0.10	±	0.13	31.5	±	4.6	0.50	±	0.30	4.6	±	0.2	9.5	±	2.2
TiO_2	0.40	±	0.20	0.33	±	0.12	0.35	±	0.09	0.31	±	0.02	0.26	±	0.05
Al_2O_3	5.8	±	1.2	3.6	±	0.7	5.0	±	1.4	9.18	±	0.09	7.4	±	1.5
Fe_{23}	3.2	±	1.22	4.6	±	1.3	7.0	±	3.9	2.33	±	0.11	2.8	±	0.6
Sb_2O_3	< LOD			1.5	±	0.5	0.4	±	0.4	3.9	±	1.5	14.8	±	2.6
SO_3	0.5	±	0.3	< LOD			0.7	±	0.4	0.5	±	0.2	0.3	±	0.3
Cl_2O	3.1	±	1.9	2.1	±	0.7	2.4	±	0.3	2.7	±	0.8	1.9	±	0.5
CoO	0.24	±	0.04	0.02	±	0.01	0.10	±	0.03	< LOD			< LOD		
P_2O_5	< LOD			0.09	±	0.07	0.14	±	0.05	< LOD			< LOD		
ZnO	0.03	±	0.01	< LOD			0.09	±	0.05	0.02	±	0.01	0.05	±	0.01
SrO	0.18	±	0.06	0.04	±	0.01	0.13	±	0.04	0.12	±	0.01	0.26	±	0.05
SnO_2	< LOD			0.22	±	0.11	< LOD			0.04	±	0.01	< LOD		
As_2O_3	< LOD			0.06	±	0.05	0.03	±	0.04	0.06	±	0.05	< LOD		
ZrO_2	0.02	±	0.01	0.08	±	0.01	< LOD			0.03	±	0.01	0.06	±	0.01

and 32.4 (face B) wt% of PbO). Moreover, as shown in the elemental composition maps, the yellow glass has the highest content of Sn, up to 0.22 and 0.28 wt% (faces A and B, respectively) of SnO_2, and the lowest of Sr and Ca, respectively down to 0.04 and 7.0 (face A) and 0.05 and 7.4 (face B) wt% of SrO and CaO. It should be noted that as Pb can also act as a stabilizer (Pinto et al. 2020), lower Ca contents are required to produce stable glasses. The blue glass presents the highest contents of Mn, Cu, and Co, respectively about 0.94 (face A) and 0.91 wt% of MnO, 0.31 (face A) and 0.27 (face B) wt% of CuO, and 0.24 (face A) and 0.21 (face B) wt% of CoO. The black glass contains up to 7.0 (face A) and 4.4 (face B) wt% of Fe_2O_3, whereas the white glass shows the highest content of Sb, up to 3.9 (eyes-face A), 4.7 (eyes-face B), 14.8 (balls-face A), and 14.1 (balls-face B) wt% of Sb_2O_3. It should be noted that, in glass matrices, the depth analyzed by XRF is strongly dependent on the energy of the X-ray photons (Colomban et al. 2021). Therefore, the obtained wt% values for heavy atoms such as Pb and Sb could be overestimated, although that would not affect the discussion of the results (Colomban et al. 2021).

According to these results (Tables 1 and 2), the composition of the different glasses presents a general good agreement between both faces, as expected taking into account that the fabrication procedure of both faces should be almost simultaneous. However, a noticeable difference is found regarding the composition of the white glass of the eyes (i.e., sclera). The eyes in face B present 25.4 wt% of CaO and 1.0 wt% of TiO_2, whereas the eyes of face A present only 11.7 wt% of CaO and 0.31 wt% of TiO_2. Thus, while the amount of Sb_2O_3 is almost constant in both cases, the eyes in face B present more than a double amount of CaO and triple of TiO_2. These differences will be further explored by combining punctual analysis with XRF and Raman spectroscopy in the next sections.

The analysis of the diverse glasses, looking forward to identifying the employed pigments or chromophores, was deepened by the study of 42 points, 20 in face A and 22 in face B, by X-ray fluorescence and Raman spectroscopy in microscopic mode. Fig. 2 shows the location of all the analyzed points, whereas Tables S.1 and S.2 (see Supplementary Information) contain the micrographs corresponding to each measurement. As mentioned before, Tables S.3 and S.4 (see Supplementary Information) include the composition measured for each point by XRF. Moreover, Figure S.3 (see Supplementary Information) includes the Raman spectra of all the studied points. Due to the extension of these datasets, a selection of representative points from each glass has been sorted out for their detailed discussion.

As evidenced in preliminary results (Pinto et al. 2020), the study of the blue glass by Raman spectroscopy does not provide information about the employed pigments or chromophores (Fig. 6.a). However, the XRF data confirmed the use of Mn, Cu, and Co at low contents as blue chromophores (Tables 1 and 2). These results are in good agreement with those of one of the glass pendants from Mozia (Sicily, Italy) (Arletti et al. 2012). On the contrary, the features of the Raman spectra of the glass network are clearly identified in this glass. The polymerization index (I_P) of this glass (Colomban et al. 2006), calculated from measurements in well-preserved areas, reached a value of 1.07 ± 0.11, in good agreement with the value 1.1 previously published in a preliminary work (Pinto et al. 2020). Areas of the blue glass with a whitish superficial alteration, such as those seen in the micrograph around point A-16 (Fig. 6.a), do not provide any information about the nature of the alteration (Figure S.3, see Supplementary Information). Likewise, the elemental composition of well-preserved and apparently altered blue areas does not differ significantly (e.g., see A-15 and A-16 in Table S.3 and Figure S.3 in the Supplementary Information).

Regarding the yellow glass (Fig. 6.b), the obtained Raman spectra not only show the broad bands corresponding to the glass network, but also expose the pigments employed to achieve this color. The obtained spectra in both faces showed bands at about 140, 336, 455, and 512 cm^{-1}, which indicated the use of a variety of the pigment known as Naples Yellow. In particular, the bands at about 455 and 512 cm^{-1} indicated the use of a pyrochloric triple oxide ($Pb_2Sb_{2-x}Sn_xO_{7-x/2}$) (Colomban 2005; Sandalinas et al. 2006). XRF data confirmed the presence of Pb, Sb, and Sn in the yellow glass (Tables 1 and 2). However, the atomic percentage of Pb, about $10.46 \pm 0.11\%$, is much higher than the combined amount of Sb and Sn, respectively of about 0.76 ± 0.01 and $0.12 \pm 0.02\%$. Therefore, it could also be expected the presence of Litharge PbO as a yellow pigment (i.e., at the temperatures employed for the glass fabrication, it cannot be expected the presence of other lead oxides) (Costantini et al. 2020), or even more probably to the presence of PbO as fluxing agent, as indicated by the ν_{max} Si-O stretching value of yellow glass, about 980 cm^{-1} (Colomban 2013). It should be noticed that the presence of the pyrochloric triple oxides has been related to a certain orange hue provided by these yellow pigments (Sandalinas et al. 2006), which can be appreciated in this sample.

This kind of compounds can be obtained from Sb_2O_3 or Sb_2S_3, but the absence of S in the yellow glass (Tables 1 and 2) indicated that, if the pyrochloric triple oxide was accidentally obtained during the glass preparation, the Sb should have been incorporated as Sb_2O_3 to the glass (Hradil et al. 2007). It is known that the use of Naples Yellow ($Pb_2Sb_2O_7$) is well-documented in ancient Egypt (1500 BC), and it has been suggested that the pigment was first obtained and then incorporated into the glass together with lead

Table 2 XRF average composition of oxides (wt%) of the glasses composing face B of the glass pendant. The LOD is about an average of ± 0.01% for trace elements. Other elements, such as Ni, and V, were not found in concentrations above the detection limit. The concentration values indicated should be taken with caution since the matrix effect has not been taken into account; they should be considered semiquantitative. Although the order of magnitude is correct

Oxide \ Glass	Blue (wt%)			Yellow (wt%)			Black (wt%)			White-Eye (wt%)			White-Ball (wt%)		
SiO_2	65.2	±	2.0	40.4	±	4.3	62.9	±	1.7	46.7	±	11.0	44.6	±	16.0
Na_2O	8.3	±	0.9	6.3	±	0.6	8.0	±	1.1	5.0	±	1.9	6.1	±	0.7
K_2O	2.0	±	0.3	2.0	±	0.4	3.2	±	0.4	2.6	±	0.4	2.2	±	0.3
CaO	13.0	±	0.5	7.4	±	1.2	12.8	±	1.4	25.4	±	10.0	9.8	±	2.0
MgO	0.59	±	0.06	0.52	±	0.08	0.66	±	0.12	0.62	±	0.04	0.5	±	0.10
MnO	0.91	±	0.09	0.04	±	0.02	0.2	±	0.2	0.44	±	0.01	0.28	±	0.08
CuO	0.27	±	0.03	0.07	±	0.01	0.17	±	0.03	0.04	±	0.01	0.04	±	0.01
PbO	0.02	±	0.01	32.4	±	4.0	0.16	±	0.18	4.8	±	1.3	9.6	±	4.3
TiO_2	0.32	±	0.02	0.33	±	0.01	0.26	±	0.06	1.0	±	0.6	0.5	±	0.3
Al_2O_3	3.1	±	0.4	2.9	±	0.3	3.3	±	0.4	3.4	±	0.5	7.1	±	5.2
Fe_2O_3	2.29	±	0.13	4.1	±	0.4	4.4	±	0.9	3.1	±	0.7	2.8	±	0.7
Sb_2O_3	0.03	±	0.02	1.5	±	0.4	0.99	±	1.03	4.7	±	0.6	14.1	±	9.8
SO_3	1.1	±	0.4	< LOD			0.77	±	0.14	0.48	±	0.02	0.5	±	0.3
Cl_2O	2.4	±	0.5	1.6	±	0.4	2.0	±	0.3	1.39	±	0.08	1.2	±	0.3
CoO	0.21	±	0.02	< LOD			0.09	±	0.05	< LOD			< LOD		
P_2O_5	0.12	±	0.05	0.13	±	0.05	0.17	±	0.08	0.22	±	0.11	0.14	±	0.14
ZnO	0.02	±	0.01	0.03	±	0.03	0.05	±	0.02	0.02	±	0.01	0.03	±	0.01
SrO	0.12	±	0.01	0.05	±	0.01	0.12	±	0.03	0.11	±	0.03	0.3	±	0.2
SnO_2	< LOD			0.28	±	0.08	0.03	±	0.02	0.04	±	-	0.13	±	0.06
As_2O_3	< LOD			0.14	±	0.03	< LOD			< LOD			< LOD		
Cr_2O_3	< LOD			< LOD			< LOD			< LOD			0.02	±	0.02
ZrO_2	< LOD			0.08	±	0.01	< LOD			0.02	±	0.02	0.09	±	0.05

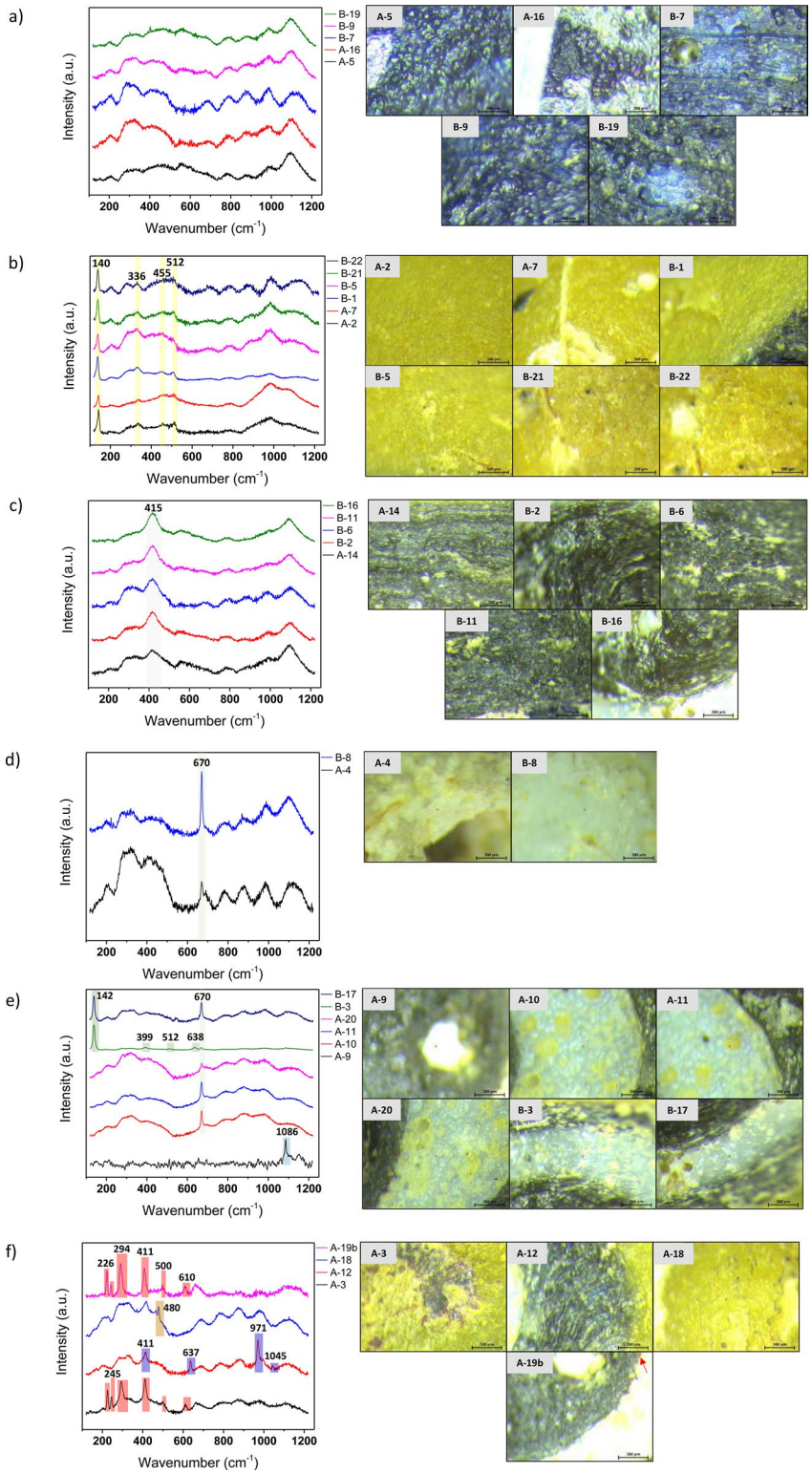

Fig. 6 Raman spectra and micrographs of the representative points analyzed from the blue (**a**), yellow (**b**), black (**c**), white-balls (**d**), white-eyes (**e**) glasses (red spot at the center indicates the XRF and Raman measurement location (see Table S.1 and Table S.2, in the Supplementary Information, for a magnified view), with the exception of point A-19b where the analyzed point is indicated by a red arrow). Raman spectra and micrographs of other points of interest (**f**). Raman bands related to the lead-based pigments are shaded in yellow (**b**). Raman band related to the Fe-S chromophore is shaded in grey (**c**). Raman band related to the calcium antimoniate is shaded in light green (d and e). Raman bands related to the titanium oxide are shaded in dark green (**e**). Raman band related to calcium carbonate is shaded in blue (**e**). Raman bands related to wollastonite, hematite, and the soda-lime glass (i.e., band at 480 cm-1, not the entire glass network spectrum) are shaded respectively in red, blue, and gold (**f**). Position of each one of the identified Raman bands are indicated in the graphs

oxides (Lahlil et al. 2010). Moreover, $Pb_2Sb_2O_7$ was identified by X-ray diffraction in older glass pieces from Mozia (Silicy, Italy) (Arletti et al. 2012). On the contrary, the controlled synthesis of pyrochloric triple oxides was initially reported from 1980, but in the last decades, clear evidence has been provided about their use in the Italian paintings from the 17th century (Hradil et al. 2007; Rosi et al. 2009). Moreover, it has been suggested the presence of pyrochloric triple oxides in Roman glass pieces (1st c. BC) (Lahlil et al. 2011), as well as identified on Egyptian Scarabs found on

the Necropolis of Vinhadas Caliças (Portugal) (6th c. BC) (Costa et al. 2019a). Moreover, one previous study on a pre-Roman glass bead recovered in Tutugi (3rd c. BC, Granada, Spain) suggested the use of Naples Yellow (Sánchez et al. 2012), although the obtained Raman spectra were virtually identical to those obtained in this work.

Modern attempts to produce this kind of pigments using traditional recipes and means have pointed out the difficulty of obtaining the desired compounds successfully. In fact, it is reported that temperatures up to 1000 ºC and calcination times of about 4–10 h could be required, being necessary sometimes successive grinding and calcination steps, without ensuring the successful obtention of a pure yellow pigment (Hradil et al. 2007). On the contrary, they found that the addition of SnO_2 to the mixture facilitates the production of yellow pigments based on pyrochloric triple oxides (Hradil et al. 2007). Therefore, it seems possible that the presence of the pyrochloric triple oxide on the studied glass pendant was intentional, as an optimization of the previous Egyptian recipe for the obtention of yellow pigments and their incorporation in glass pieces. It should be noticed that the identification of the pyrochloric triple oxide in this work provides one of the earliest evidence of their use, intentional or accidental, in history.

The black glass (Fig. 6.c) shows a very strong band at 415 cm^{-1}, which has been previously attributed to the Fe-S chromophore (Tournié et al. 2012). This chromophore was traditionally used to produce amber glass, but in sufficient concentrations, it appears black. The formation of this chromophore in silicate glass requires the presence of iron oxides and sulfur species in the glass melt (Prinsloo and Colomban 2008). In fact, the black glass shows the highest amounts of Fe (about 7.0 (face A) and 4.4 (face B) wt% of Fe_2O_3) and amounts of S higher than on the yellow and white glasses (about 0.7 (face A) and 0.8 (face B) wt% of SO_3) (Tables 1 and 2). Moreover, a preliminary work evidenced the presence of hematite as iron source in the black areas (Pinto et al. 2020), which presence is also confirmed in this work (see Fig. 6.f). The obtained results present no difference between the black glass of the pupils, eye-lines, or eye-browns.

On the contrary, unexpected differences are found in the white glass. The analysis of the white balls by Raman spectroscopy evidenced the use of calcium antimoniate ($CaSb_2O_6$, band at 670 cm^{-1}) as a white pigment (Fig. 6.d) (Pinto et al. 2020), in good agreement with the XRF results showing the highest amount of Sb on these elements (about 14.8 and 14.1 wt% of Sb_2O_3 for faces A and B, respectively). The sclera of the eyes of face A present similar Raman spectra (Fig. 6.e), evidencing the presence of calcium antimoniate by the band at 670 cm^{-1}, although the Sb_2O_3 concentration measured by XRF is only about 3.9 wt%. On the contrary, the sclera of the eyes of face B shows not only the presence of calcium antimoniate (4.8 wt% of Sb_2O_3), but also of anatase (TiO_2, bands at 142, 399, 512, and 638 cm^{-1}) (Prinsloo and Colomban 2008). This interpretation is also supported by the XRF results (Tables 1 and 2), with the eyes of face B showing higher amounts of TiO_2 (1.0 wt%) than those of face A (0.31 wt% of TiO_2). Another difference between the composition of the white glass from the decorative balls and those of the eyes is related to the PbO contents, which are higher in the balls (about 9.5–10.0 wt%) than in the eyes (about 4.5-5.0 wt%). It should also be noted that the sclera of face B also shows an anomalously high amount of CaO (25.4 wt%), which could be related to the presence of calcium carbonate as a surface alteration (see Fig. 2, where it is clearly appreciated a noticeable alteration of the eyes in face B) (Zanini et al. 2023b). This kind of alteration (i.e., carbonatation) is also clearly visible in the XRF mapping data (Fig. 5), which shows a high concentration of Ca on the alterations present around the nose. In particular, the analyzed point 21 of face A corresponds to those alterations, being its composition dominated by CaO (75.2 wt%, see Table S.3, Supporting Information).

Moreover, the white spots which appear to mimic the brightness of the pupils on face A are also identified as calcium carbonate ($CaCO_3$, main band at 1086 cm^{-1}) (Fig. 6.e) (Ricciardi et al. 2009), showing a CaO content of 86.0 wt% (analyzed point 9 of face A, see Table S.3, Supporting Information). Although it cannot be discarded that these with spots also correspond to alterations, their similar positions in the eyes could suggest that they were intentionally placed on top of the glass eyes during their manufacturing as an artistic feature. However, further work is required to confirm this hypothesis.

The presence of two or even three potentially different white glass compositions, particularly significant on the pre-made eyes, as well as the differences regarding the elaboration of the pendant with these glasses (see Fig. 4 and corresponding discussion), suggests the production of the glass pendant in a secondary workshop. It can be expected that the craftsman responsible for its manufacture received different batches of primary white glass, employing them indistinctly to produce the pendant. This interpretation would be in good agreement with established theories about the production and distribution of glass in the Mediterranean at that time (Seefried 1982; Dubin 2009; Gratuze 2013). Moreover, it should be highlighted the identification of anatase (TiO_2) as a potential white pigment employed at that time, encouraging the debate about its not-so-recent use as a white pigment, although its intentional addition to the glass cannot be ensured (Edwards et al. 2006). In addition, the presence of $CaSb_2O_6$ and the absence of $Ca_2Sb_2O_7$ indicate that the glass was produced at temperatures below 1100 °C (i.e., $Ca_2Sb_2O_7$ is formed from $CaSb_2O_6$ when the glass was

produced at temperatures about or over 1100 °C) (Costa et al. 2019b).

Finally, it is possible to discuss additional remarks highlighting other relevant features of the obtained Raman spectra (Fig. 6.f, point A-3). First, the study of a black alteration detected in face A has provided a clear identification of hematite (Fe_2O_3, bands at 226, 245, 294, 411, 500, and 610 cm^{-1}) (Pinto et al. 2020). While the same component has been found in a small reddish spot seen on the outer border of the black pupil (Fig. 6.f, point A-19b), confirming the presence of hematite as an iron source in the black glass composition. Moreover, a few spectra (Fig. 6.f, point A-18) show a small band about 480 cm^{-1} over the glass network Raman spectra. This band has been previously detected and identified as typical in soda-lime glasses, and no additional information is provided in this case (Neuville and Mysen 1996; Ben Kacem et al. 2017). In addition, it was possible to detect the presence of wollastonite ($CaSiO_3$) in the black glass (Fig. 6.f, point A-12), evidenced by the bands at 411, 637, 971, and 1045 cm^{-1} (Colomban 2019). Interestingly, this spectrum corresponds to the β-phase of wollastonite, indicating that temperatures over 1120 °C were not achieved during the manufacturing process (Zhu and Sohn 2012; Colomban 2019).

It should be noticed that the polymerization index previously determined for the blue glass is related to maximum firing temperatures of about 1100 °C (Colomban et al. 2004), in good agreement with this maximum temperature determined from the mineralogical composition determined for both the white and black glass. Therefore, the fabrication process of the glass pendant, including the diverse glass compositions, firing temperature, and fabrication steps, has been clearly identified in this work.

Conclusions

The non-destructive multi-analytical study performed on a unique Phoenician glass masterpiece from the 2nd -1st centuries BC found on the Vaccaean necropolis of "Las Ruedas" (archaeological site of Pintia, Valladolid, Spain) has revealed most of the details regarding their fabrication. As the first highly detailed study on this kind of pre-Roman glass pieces, this work evidenced that their study using the proposed multi-analytical approach would be essential to confirm the main glass workshops and trade routes at that age, as the high specialization required to produce such pieces and their scarcity suggest the existence of a few production centers.

The studied glass pendant is a cylindrical glass bead, recovered in 2007 from the tomb of a high-rank young woman suspected of proceeding from the Iberian culture. The pendant corresponds to the F_1 classification proposed by M. Seefried, being one of the very few well-preserved and recovered in a closed context. Moreover, it is the pendant of this type recovered further west of the Mediterranean region, while the highest number of these pendants have been recovered from the Caucasus and nearby regions.

X-ray tomography's study of the pendant provided unknown evidence about its fabrication route. These pieces were known to be fabricated by adding melt drops of the diverse colored glasses. However, the well-defined geometrical features of the eyes, composed of the pupil and sclera, contradicted that route. The eyes should have been produced by casting using hemispherical molds, and then placed into the pendant, as confirmed by the distribution of each glass, clearly visible in the cross-sections of the 3D tomographic reconstruction, and the deformation of the gas bubbles within the surrounding glasses. Moreover, although it was previously believed that the nose was modeled from the yellow glass of the face, it has been proved that it was added after placing the eyes and the eyebrows.

The microchemical analysis of the pendant performed by X-ray fluorescence and Raman spectroscopy, both in microscopic mode, suggested that the main composition of the glasses corresponds to the so-called low magnesium soda-lime silica glass obtained using natron as a fluxing agent. Moreover, the presence of some surface alterations due to carbonatation processes was evidenced by the elemental mapping of both faces by XRF. The detailed analysis of the composition of each glass revealed the diverse chromophores or pigments employed, as well as reasonable homogeneity among each glass throughout the entire piece, with one significant exception for the white glasses. The white balls placed in the top and bottom of the pendant, as well as the sclera of the eyes of face A, present $CaSb_2O_6$ as a pigment, while the analysis by XRF and Raman spectroscopy of the sclera of the eyes of face B also evidenced the presence of TiO_2 as white pigment. The probable use of different white glasses in the same piece suggests its production in a secondary workshop from primary white glass ingots regardless of their origin and composition.

As mentioned, the other glasses are homogeneous regarding the use of pigments or chromophores. The blue hue is achieved by using Mn, Cu, and Co, typically found in contemporary blue Phoenician glasses. The black hue is attributed to Fe-S chromophore, achieved by adding iron oxides and sulfur species to the glass melt, as suggested by the Raman spectra, the presence of higher S contents, and the detection of hematite remains by Raman spectroscopy. Finally, the yellow hue is achieved by using a variety of the pigment known as Naples Yellow, a pyrochloric triple oxide ($Pb_2Sb_{2-x}Sn_xO_{7-x/2}$). The intentional or accidental use of this pigment cannot be ensured, although the complexity

of its production could hinder its accidental origin. In any case, this could be one of the earliest evidence of their use in history.

Additionally, the detailed point-by-point microchemical characterization performed confirmed the presence of $CaSb_2O_6$ and the absence of $Ca_2Sb_2O_7$, as well as the presence of only the β-phase of $CaSiO_3$, both indicating firing temperatures below 1100 °C, which were in good agreement with those estimated from the Raman spectra features of the glass matrix.

Supplementary Information The online version contains supplementary material available at https://doi.org/10.1007/s12520-024-02062-w.

Acknowledgements This work has been financially supported by the Regional Government of Castilla y León and the EU-FEDER program (CLU-2019-04 and VA210P20), MCIN/AEI/https://doi.org/10.13039/501100011033 and the EU NextGenerationEU/PRTR program (PLEC2021-007705), and MCIN/AEI/https://doi.org/10.13039/501100011033/ and FEDER "Una manera de hacer Europa" (PID2022- 142495NB-I00). Also, the authors acknowledge the TEMPOS Vega Sicilia group (Valladolid, Spain) for the patronage of the "Centro de Estudios Vacceos Federico Wattenberg".

Author contributions S. B. S. wrote the main manuscript text. S. B. S., E. E., J. A., E. R., and J. P. carried out the research and experiments. C. S. M., A. C. P., J. M. M., and J. P. designed the study methodology, supervised the work, and reviewed the manuscript. J. A. also reviewed the manuscript. C. S. M. provided access to the sample under study. C. S. M., A. C. P., and J. P. obtained the funding.

Funding Open Access funding provided thanks to the CRUE-CSIC agreement with Springer Nature.

Data availability No datasets were generated or analysed during the current study.

Declarations

Competing interests The authors declare no competing interests.

References

Arletti R, Ferrari D, Vezzalini G (2012) Pre-roman glass from Mozia (Sicily-Italy): the first archaeometrical data. J Archaeol Sci 39:3396–3401. https://doi.org/10.1016/j.jaS.2012.06.009

Ávila JJ (2011) Los Objetos De Vidrio Procedentes Del Yacimiento De Pajares: Estudio Preliminar. Memorias Arqueol Extrem 3:139–151

Ben Kacem I, Gautron L, Coillot D, Neuville DR (2017) Structure and properties of lead silicate glasses and melts. Chem Geol 461:104–114. https://doi.org/10.1016/j.chemgeo.2017.03.030

Bertini M, Mokso R, Krupp EM (2014) Unwinding the spiral: discovering the manufacturing method of Iron Age Scottish glass beads. J Archaeol Sci 43:256–266. https://doi.org/10.1016/j.jaS.2014.01.001

Bettineschi C, Angelini I, Malaman E, Gratuze B (2020) Composizione E provenienza dei vetri punici dalla necropoli di Nora. Quad Norensi 8:231–240

Bouchard M, Smith DC (2003) Catalogue of 45 reference Raman Spectra of minerals concerning research in art history or archaeology, especially on corroded metals and coloured glass. Spectrochim Acta - Part Mol Biomol Spectrosc 59:2247–2266. https://doi.org/10.1016/S1386-1425(03)00069-6

Čelhar M, Kukoc S (2014) Stakleni privjesak u obliku ljudske glave iz Nadina. Prilog Poznavanju importa u kulturi Liburna - Glass head pendant from Nadin. A contribution to the understanding of import in the liburnian culture. Pril Instituta Za Arheol u Zagreb 31:89–100

Cheng Q, Zhang X, Guo J et al (2019) Application of computed tomography in the analysis of glass beads unearthed in Shanpula cemetery (Khotan), Xinjiang Uyghur Autonomous Region. Archaeol Anthropol Sci 11:937–945. https://doi.org/10.1007/s12520-017-0582-6

Colomban P (2003) Polymerization degree and Raman identification of ancient glasses used for jewelry, ceramic enamels and mosaics. J Non Cryst Solids 323:180–187. https://doi.org/10.1016/S0022-3093(03)00303-X

Colomban P (2005) Case Study: glasses, glazes and ceramics – Recognition of Ancient Technology from the Raman Spectra. In: Edwards HGM, Chalmers JM (eds) Raman Spectroscopy in Archaeology and Art History. RSC Analytical Spectroscopy Monographs, Cambridge, pp 192–205

Colomban P (2013) Non-destructive Raman analysis of ancient glasses and glazes. Mod Methods Anal Archaeol Hist Glas I 1:275–300. https://doi.org/10.1002/9781118314234.ch12

Colomban P (2019) Supplementary information for Raman Spectroscopy in Archaeology and Art History Colouring agents for Glass. Tracing Innovation and Exchange Routes, Glaze and Enamel

Colomban P, Treppoz F (2001) Identification and differentiation of ancient and modern European porcelains by Raman macro- and micro-spectroscopy. J Raman Spectrosc 32:93–102. https://doi.org/10.1002/jrs.678

Colomban P, Milande V, Le Bihan L (2004) On-site Raman analysis of Iznik pottery glazes and pigments. J Raman Spectrosc 35:527–535. https://doi.org/10.1002/jrS.1163

Colomban P, Tournie A, Bellot-Gurlet L (2006) Raman identification of glassy silicates used in ceramics, glass and jewellery: a tentative differentiation guide. J Raman Spectrosc 37:841–852. https://doi.org/10.1002/jrS.1515

Colomban P, Gironda M, Edwards HGM, Mesqui V (2021) The enamels of the first (soft-paste) European blue-and- white porcelains: Rouen, Saint-Cloud and Paris factories: complementarity ofRaman and X-ray fluorescence analyses with mobile instruments to identify the cobalt ore. J Raman Spectrosc 52:2246–2261

Constantinescu B, Cristea-Stan D, Szőkefalvi-Nagy Z et al (2018) PIXE and PGAA – complementary methods for studies on ancient glass artefacts (from byzantine, late medieval to modern Murano glass). Nucl Instruments Methods Phys Res Sect B Beam Interact Mater Atoms 417:105–109. https://doi.org/10.1016/j.nimb.2017.07.017

Costa M, Arruda AM, Barbosa R et al (2019a) A micro-analytical study of the scarabs of the necropolis of vinha das caliças (Portugal). Microsc Microanal 25:214–220. https://doi.org/10.1017/S143192761801560X

Costa M, Arruda AM, Dias L et al (2019b) The combined use of Raman and micro-X-ray diffraction analysis in the study of archaeological glass beads. J Raman Spectrosc 50:250–261. https://doi.org/10.1002/jrs.5446

Costa M, Barrulas P, Dias L et al (2019c) Multi-analytical approach to the study of the European glass beads found in the tombs of Kulumbimbi (Mbanza Kongo, Angola). Microchem J 149:103990. https://doi.org/10.1016/j.microc.2019.103990

Costa M, Barrulas P, Arruda AM et al (2021) An insight into the provenance of the phoenician-punic glass beads of the necropolis of Vinha das Caliças (Beja, Portugal). Archaeol Anthropol Sci 13. https://doi.org/10.1007/s12520-021-01390-5

Costantini I, Lottici PP, Castro K, Madariaga JM (2020) Use of temperature controlled stage confocal raman microscopy to study phase transition of lead dioxide (Plattnerite). Minerals 10:1–19. https://doi.org/10.3390/min10050468

Devulder V, Gerdes A, Vanhaecke F, Degryse P (2015) Validation of the determination of the B isotopic composition in roman glasses with laser ablation multi-collector inductively coupled plasma-mass spectrometry. Spectrochim Acta - Part B Spectrosc 105:116–120. https://doi.org/10.1016/j.sab.2014.08.038

Dong J, Li Q, Hu Y (2020) Multi-technique analysis of an ancient stratified glass eye bead by OCT, μ-XRF, and μ-Raman spectroscopy. Chin Opt Lett 18:090001. https://doi.org/10.3788/col202018.090001

Dubin LS (2009) The History of Beads: From 100,000 B.C. to the Present. Abrams

Edwards HGM, Nik Hassan NF, Middleton PS (2006) Anatase-a pigment in ancient artwork or a modern usurper? Anal Bioanal Chem 384:1356–1365. https://doi.org/10.1007/s00216-005-0284-2

Franceschin G, Zanini R, Iori G et al (2024) Non-destructive 3D exploration of silicate glass corrosion: a combined multiscale approach from the macro to the nanoscale. Phys Chem Chem Phys 26:9697–9707. https://doi.org/10.1039/d3cp05221d

García-Heras M, Rincón JM, Jimeno A, Villegas MA (2005) Pre-roman coloured glass beads from the Iberian Peninsula: a chemico-physical characterisation study. J Archaeol Sci 32:727–738. https://doi.org/10.1016/j.jaS.2004.12.007

Gratuze B (2013) Provenance analysis of Glass artefacts. Mod Methods Anal Archaeol Hist Glas I 1:311–343. https://doi.org/10.1002/9781118314234.ch14

Henderson J, Henderson J (2013) Glass Chemical Compositions

Hradil D, Grygar T, Hradilová J et al (2007) Microanalytical identification of Pb-Sb-Sn yellow pigment in historical European paintings and its differentiation from lead tin and Naples yellows. J Cult Herit 8:377–386. https://doi.org/10.1016/j.culher.2007.07.001

Jokubonis C, Wobrauschek P, Zamini S et al (2003) Results of quantitative analysis of celtic glass artefacts by energy dispersive X-ray fluorescence spectrometry. Spectrochim Acta - Part B Spectrosc 58:627–633. https://doi.org/10.1016/S0584-8547(02)00289-6

Lahlil S, Biron I, Cotte M et al (2010) Synthesis of calcium antimonate nano-crystals by the 18th dynasty Egyptian glassmakers. Appl Phys Mater Sci Process 98:1–8. https://doi.org/10.1007/s00339-009-5454-1

Lahlil S, Cotte M, Biron I et al (2011) Synthesizing lead antimonate in ancient and modern opaque glass. J Anal Spectrom 26:1040–1050. https://doi.org/10.1039/c0ja00251h

Malaman E, Bettineschi C, Angelini I et al (2024) Phoenician head pendants: Contextualizing archaeological and collection pieces. In: DAT@ MI. p 36

Mathis F, Othmane G, Vrielynck O et al (2010) Combined PIXE/PIGE and IBIL with external beam applied to the analysis of Merovingian glass beads. Nucl Instruments Methods Phys Res Sect B Beam Interact Mater Atoms 268:2078–2082. https://doi.org/10.1016/j.nimb.2010.02.058

Medeghini L, Botticelli M, Cadena-Irizar AC et al (2022) Blue shadows of roman glass artefacts. Microchem J 179:107526. https://doi.org/10.1016/j.microc.2022.107526

Micheletti F, Orsilli J, Melada J et al (2020) The role of IRT in the archaeometric study of ancient glass through XRF and FORS. Microchem J 153:104388. https://doi.org/10.1016/j.microc.2019.104388

Neuville DR, Mysen BO (1996) Role of aluminium in the silicate network: in situ, high-temperature study of glasses and melts on the join SiO2-NaAlO2. Geochim Cosmochim Acta 60:1727–1737. https://doi.org/10.1016/0016-7037(96)00049-X

Nykonenko D, Yatsuk O, Guidorzi L et al (2023) Glass beads from a scythian grave on the island of Khortytsia (Zaporizhzhia, Ukraine): insights into bead making through 3D imaging. Herit Sci 11:1–19. https://doi.org/10.1186/s40494-023-01078-0

Oikonomou A, Triantafyllidis P, Beltsios K et al (2008) Raman structural study of ancient glass artefacts from the island of Rhodes. J Non Cryst Solids 354:768–772. https://doi.org/10.1016/j.jnoncrysol.2007.08.092

Pinakidou F, Katsikini M, Paloura EC et al (2020) Transition metal chromophores in glass beads of the classical and hellenistic period: bonding environment and colouring role. Spectrochim Acta - Part B Spectrosc 171:105928. https://doi.org/10.1016/j.sab.2020.105928

Pinto J, Prieto AC, Coria-Noguera JC et al (2020) Investigating glass beads and the funerary rituals of ancient Vaccaei culture (S. IV-I BC) by Raman spectroscopy. J Raman Spectrosc 1–16. https://doi.org/10.1002/jrs.6049

Prinsloo LC, Colomban P (2008) A Raman spectroscopic study of the Mapungubwe oblates: glass trade beads excavated at an Iron Age archaeological site in South Africa. J Raman Spectrosc 39:79–90. https://doi.org/10.1002/jrS.1816

Quartieri S, Riccardi MP, Messiga B, Boscherini F (2005) The ancient glass production of the medieval Val Gargassa glasshouse: Fe and Mn XANES study. J Non Cryst Solids 351:3013–3022. https://doi.org/10.1016/j.jnoncrysol.2005.06.046

Ricciardi P, Colomban P, Tournié A et al (2009) A non-invasive study of roman age mosaic glass tesserae by means of Raman spectroscopy. J Archaeol Sci 36:2551–2559. https://doi.org/10.1016/j.jaS.2009.07.008

Rolland J, Venclová N (2021) Iron Age glass-working in Moravia, Central Europe: new archaeometric research on raw glass and waste — 3rd–first century BC. Archaeol Anthropol Sci 13:1–19. https://doi.org/10.1007/s12520-021-01374-5

Rosi F, Manuali V, Miliani C et al (2009) Raman scattering features of lead pyroantimonate compounds. Part I: XRD and Raman characterization of Pb2Sb2O7 doped with tin and zinc. J Raman Spectrosc 40:107–111. https://doi.org/10.1002/jrS.2092

Rosi F, Manuali V, Grygar T et al (2011) Raman scattering features of lead pyroantimonate compounds: implication for the non-invasive identification of yellow pigments on ancient ceramics. Part II. In situ characterisation of Renaissance plates by portable micro-raman and XRF studies. J Raman Spectrosc 42:407–414. https://doi.org/10.1002/jrS.2699

Sánchez A, Tuñón J, Parras D (2012) Micro Raman spectroscopy (MRS) and energy dispersive x-ray micro fluorescence (μEDXRF) analysis of pigments in the Iberian cemetery of Tutugi (from the fourth to the third century BC, Galera, Granada, Spain). J Raman Spectrosc 43:1788–1795. https://doi.org/10.1002/jrS.4080

Sandalinas C, Ruiz-Moreno S, López-Gil A, Miralles J (2006) Experimental confirmation by Raman spectroscopy of a Pb–Sn–Sb triple oxide yellow pigment in sixteenth-century Italian pottery. J Raman Spectrosc 37:1146–1153. https://doi.org/10.1002/S.1580

Sanz-Minguez C, Coria-Noguera JC (2018) La Tumba 144 de la necrópolis de las ruedas. In: Sanz-Minguez C, Blanco-Garcia JF (eds) Novedades arqueológicas en cuatro ciudades vacceas: Dessobriga, Intercatia, Pintia Y Cauca. Centro de Estudios Vacceos Federico Wattenberg de la Universidad de Valladolid, pp 129–156

Seefried M (1979) Glass Core pendants found in the Mediterranean Area. J Glass Stud 21:17–26

Seefried M (1982) Les pendentifs en verre sur noyau des pays de la Méditerranée antique. 234

Šmit, Laharnar B, Turk P (2020) Analysis of prehistoric glass from Slovenia. J Archaeol Sci Rep 29. https://doi.org/10.1016/j.jasrep.2019.102114

Tournié A, Prinsloo LC, Colomban P (2012) Raman classification of glass beads excavated on Mapungubwe hill and K2, two archaeological sites in South Africa. J Raman Spectrosc 43:532–542. https://doi.org/10.1002/jrS.3069

Truffa M, Gratuze B, Ozainne S et al (2019) A phoenician glass eye bead from 7th – 5th c. cal BCE Nin-Bèrè 3, Mali : compositional characterisation by LA – ICP – MS. J Archaeol Sci Rep 24:748–758. https://doi.org/10.1016/j.jasrep.2019.02.032

Van Strydonck M, Gratuze B, Rolland J, De Mulder G (2018) An archaeometric study of some pre-roman glass beads from Son Mas (Mallorca, Spain). J Archaeol Sci Rep 17:491–499. https://doi.org/10.1016/j.jasrep.2017.12.003

Wang D, Wen R, Henderson J et al (2020) The chemical composition and manufacturing technology of glass beads excavated from the Hetian Bizili site, Xinjiang. Herit Sci 8:1–15. https://doi.org/10.1186/s40494-020-00469-x

Zanini R, Franceschin G, Cattaruzza E et al (2023a) Compositional changes by SIMS and XPS analyses on fresh and aged roman-like glass. J Non Cryst Solids 612:122356. https://doi.org/10.1016/j.jnoncrysol.2023.122356

Zanini R, Franceschin G, Cattaruzza E, Traviglia A (2023b) A review of glass corrosion: the unique contribution of studying ancient glass to validate glass alteration models. Npj Mater Degrad 7:1–17. https://doi.org/10.1038/s41529-023-00355-4

Zhang X, Lei Y, Cheng Q, Zhou G (2020) Application of computed tomography in the analysis of the manufacture of eye beads technique. Microchem J 156. https://doi.org/10.1016/j.microc.2020.104798

Zhu L, Sohn HY (2012) Growth of 2 M-wollastonite polycrystals by a partial melting and recrystallization process for the preparation of high-aspect-ratio particles. J Ceram Sci Technol 3:169–180. https://doi.org/10.4416/JCST2012-00032